2014

Synthesis and electrochemical properties of WO3/C for lithium ion batteries

Hong Gao
Hubei University

Shuijin S. Yang
Hubei University

Chuanqi Feng
Hubei University, University of Wollongong

Jiazhao Wang
University of Wollongong, jiazhao@uow.edu.au

Zaiping Guo
University of Wollongong, zguo@uow.edu.au

Publication Details

Gao, H., Yang, S., Feng, C., Wang, J. & Guo, Z. (2014). Synthesis and electrochemical properties of WO3/C for lithium ion batteries. ECS Transactions, 62 (1), 9-18.

Synthesis and electrochemical properties of WO3/C for lithium ion batteries

Abstract
WO_3/C nanorods were prepared by a combination of hydrothermal synthesis method and the solid phase reaction method, using $(NH_4)_{10}H_2(W_2O_7)_6$, $H_2C_2O_4{\cdot}2H_2O$ and glucose(carbon source) as raw materials. The effects of different proportions of glucose on the morphologies and electrochemical properties of the final products were systematically investigated. The results showed that the WO_3/C nanorods prepared with the 10 wt.% glucose as carbon source exhibited the highest reversible specific capacity (807 mAh g^{-1}) at current density of 50 mA g^{-1} and the best cycle performances among all samples. Besides, it behaved good rate performance. It indicated that WO_3/C nanorods could be promising electrode materials for lithium ion battery application.

Keywords
ion, lithium, c, electrochemical, wo3, synthesis, properties, batteries

Disciplines
Engineering | Physical Sciences and Mathematics

Publication Details
Gao, H., Yang, S., Feng, C., Wang, J. & Guo, Z. (2014). Synthesis and electrochemical properties of WO3/C for lithium ion batteries. ECS Transactions, 62 (1), 9-18.

ECS Transactions, 62 (1) 9-18 (2014)
10.1149/06201.0009ecst ©The Electrochemical Society

Synthesis and Electrochemical Properties of WO_3/C for Lithium Ion Batteries

Hong Gao[a] , Shuijin Yang[b], Chuanqi Feng[a*] , Jiazhao Wang[c], Zaiping Guo[a,c*]

[a] Hubei Collaborative Innovation Center for Advanced Organic Chemical Materials Hubei University, Wuhan ,430068, P.R. China
[b] Hubei Key Laboratory of Pollutant Analysis & Reuse Technology, Hubei Normal University, Huangshi 435002,China
[c] Institute for Superconducting & Electronic Materials, University of Wollongong, NSW 2522, Australia

Abstract: WO_3/C nanorods were prepared by a combination of hydrothermal synthesis method and the solid phase reaction method, using $(NH_4)_{10}H_2(W_2O_7)_6$, $H_2C_2O_4 \cdot 2H_2O$ and glucose(carbon source) as raw materials. The effects of different proportions of glucose on the morphologies and electrochemical properties of the final products were systematically investigated. The results showed that the WO_3/C nanorods prepared with the 10 wt.% glucose as carbon source exhibited the highest reversible specific capacity (807 mAh g^{-1}) at current density of 50 mA g^{-1} and the best cycle performances among all samples. Besides, it behaved good rate performance. It indicated that WO_3/C nanorods could be promising electrode materials for lithium ion battery application.

1. Introduction

The need for high-performance rechargeable batteries for portable electronic devices has led to the development of lithium-ion battery (LIB). Li-ion batteries (LIBs) are considered as important power sources for the future. Such as electric cars, hybrid electric vehicles (HEVs) have prompted numerous research efforts toward developing new high-performance electrode materials for next-generation LIBs(1-2). In recent years, a world-wide effort has been made to find less expensive and environmentally benign transition metal oxides. As an important n-type semiconductor, WO_3 was used in a wide variety of applications such as chemical sensors, photocatalysis and smart windows(3). The width of band gap (2.6eV) makes WO_3 as an ideal candidate for electronics and nanodevice applications(4). It has large theoretical capacity (~700 mAh g^{-1}), low cost, enhanced safety because of its high melting temperature and mechanical stability. Besides, a very high volumetric capacity can be expected considering its high theoretical density of 7.61 g cm^{-3}. Nevertheless, WO_3 as an anode material suffers from large structural and volume variation during the charge/discharge processes, which lead to mechanical disintegration and the loss of electrical connection between the active material and current collector, severely decreasing the cycling ability of electrodes. But there are few reports on application of nano-WO_3 in the Li-ion battery. Previously, Kumagai et al. have shown that monoclinic WO_3 dense particles obtained by moderate heating of H_2WO_4 exhibited enhanced cycling performance (5-9). Since the electrode materials react with lithium

by an intercalation mechanism, the diffusion of Li^+ in the host lattice plays an important role. In consequence, the morphological characteristics of the materials are regarded as particularly important in affecting their electrochemical properties, and the morphology strongly depends on the preparation method and condition (10-20). Recently, much attention has been paid to controlling the shape and size of the nanoparticles (21-26).

In this work, WO_3/C nanorods composite was prepared by a combination of hydrothermal synthesis method and the solid phase reaction method, using $(NH_4)_{10}H_2(W_2O_7)_6$, $H_2C_2O_4 \cdot 2H_2O$ and different proportions of glucose as reactants. The electrochemical performances of WO_3/C as an anode material for the lithium ion battery were investigated. The outstanding electrochemical properties of the WO_3/C suggested that WO_3 nanorods could be a promising anode material for applications of lithium ion battery in the near future.

2. Experimental

2.1. Synthesis and characterization of the samples

All chemicals were of analytical grade and were used without further purification. The WO_3/C composite was prepared by using $(NH_4)_{10}H_2(W_2O_7)_6$, $H_2C_2O_4 \cdot 2H_2O$ (in molar ratio of 1:3) and glucose (10 wt .%, 20 wt.% and 30 wt.% to WO_3 respectively) as reactants. The glucose was used as the carbon source, which was expected to generate the carbon coating in the final product（WO_3） to obtain the WO_3/C composite. In a typical experimental procedure, $(NH_4)_{10}H_2(W_2O_7)_6$ and $H_2C_2O_4 \cdot 2H_2O$ were dissolved in 20 ml deionized water and kept stirring for 30 min , 10 ml polyethylene glycol was added dropwise in the above solution under stirring vigorously and kept stirring 5 min. The solution was then transferred into a Teflon-lined stainless steel autoclave and heated at 180 ℃ for 24 h, then cooled down to room temperature naturally. The product was collected, washed with deionized water and ethanol, and dried in air at 80 ℃. Then WO_3 and different weight ratio of glucose (10wt .%, 20wt.% and 30wt.% to WO_3 respectively) were dissolved in ethanol and kept stirring for 10 min, then dried in oven at 70 ℃ in the open air. After that the precursor was heated in a tubular furnace at 600 ℃ under Argon atmosphere for 5 hours, and then cooled slowly to the ambient temperature, marked as WO_3/C-10, WO_3/C-20 and WO_3/C-30, respectively.

The crystal structure of the WO_3/C composite was characterized by X-ray diffraction (XRD) using Cu K_α radiation (Bruker AXS, D8 diffractometer). The morphologies of the samples were observed by scanning electron microscopy (SEM; JSM, 7100F). Raman measurements were taken at room temperature on a Jobin Yvon HR800 Raman spectrometer attached to a CCD camera, with an Ar^+ laser (514.4 nm) as the excitation source.

2.2. Electrochemical measurements

Electrochemical performances of the products were tested in a model test cell system. Positive electrodes were prepared by pressing a mixture of the active material (65%), acetylene black (25%), and polytetrafluoroethylene (PTFE) (10%) onto a nickel grid. Prior to being used, the electrodes were dried at 125 ℃ in a vacuum furnace for 24 h. The electrolyte was a solution of l M $LiPF_6$ in ethylene carbonate (EC) and diethyl carbonate (DEC) (1:1 by volume). The separator was Celgard 2400 porous polypropylene. The counter and reference electrodes were lithium foil. The model test cells were assembled in an argon-filled glove box. Charge-discharge tests were carried out at different current densities in the range of 0.01 V to 3.00 V. Electrochemical impedance spectroscopy (EIS) experiments were conducted in the frequency range of 0.01-100 kHz using a CHI 600A electrochemical work station.

3. Results and discussion

3.1. Structure and morphology characterization

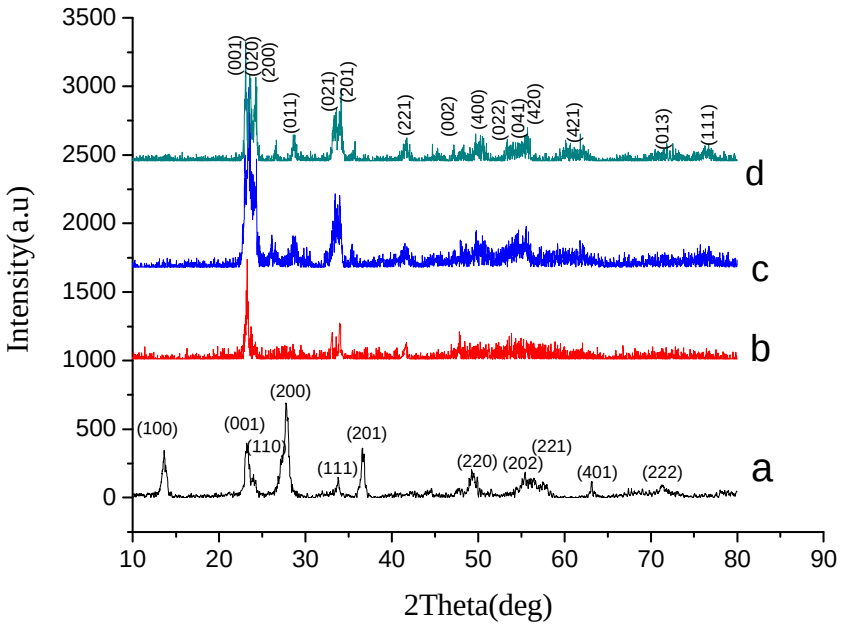

Fig 1. XRD patterns of the four samples: WO_3(a), WO_3/C-10(b), WO_3/C-20(c) and WO_3/C-30(d).

Fig 1. shows the XRD pattern of the WO_3, WO_3/C-10, WO_3/C-20 and WO_3/C-30 samples. The peaks of WO_3(a) can be well indexed to orthorhombic phase of WO_3 (JCPDS# 75-2187), with lattice constants a=7.304Å，c=3.888 Å. Whereas, the peaks of WO_3/C-10(b), WO_3/C-20(c) and WO_3/C-30(d) can be well indexed to monoclinic phase of WO_3 (JCPDS# 75-2072). In WO_3/C-20 and WO_3/C-30 composites, the peak of carbon at about 26° is observed. No other impurity peaks were detected on the XRD patterns. With the increase of the carbon source, the

diffraction peaks gets sharper. It indicates the enhancement of the crystallinity. It can be proved that the WO_3, WO_3/C-10, WO_3/C-20 and WO_3/C-30 samples were synthesized successfully by this method.

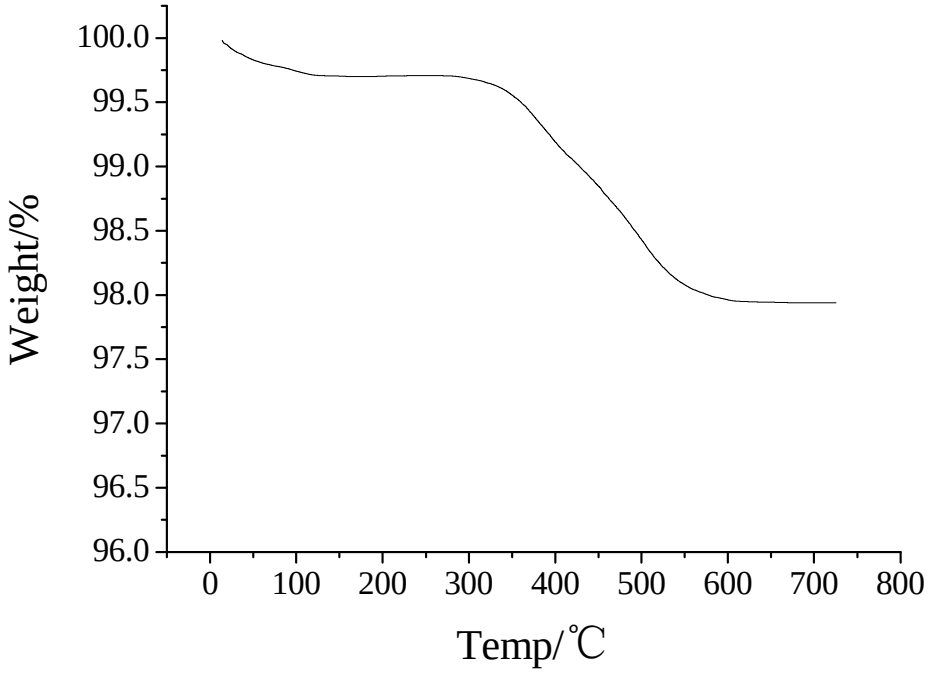

Fig 2. TG curves of WO_3/C-10 composite.

The TG curve of the WO_3/C-10 composite is shown in Fig 2. It can be seen that from 400 to 600□, the carbon was oxidized, and part of the weight of the composite was lost. Over the temperature of 600□, WO_3 was very stable. From the TG curve, the carbon content in the composite is about 2.16%.

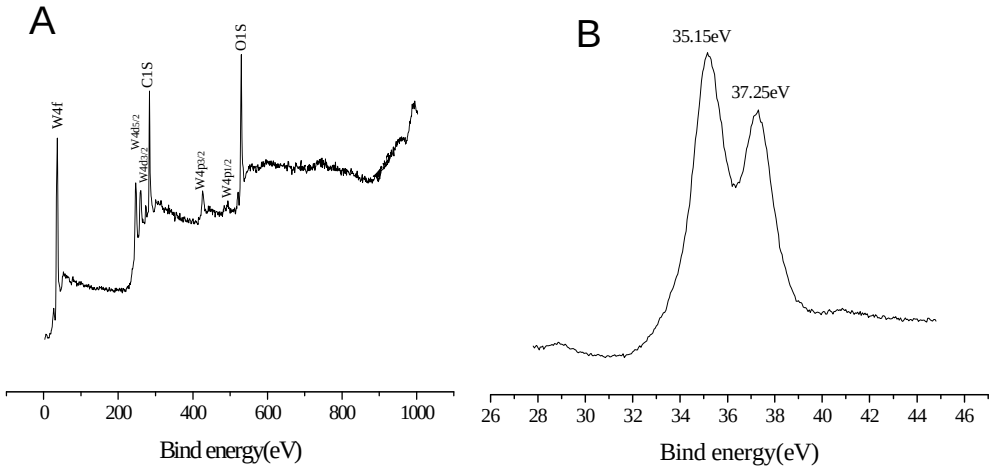

Fig 3. XPS of WO_3/C-10 composite

The XPS of WO_3/C-10 composite is shown in Fig 3. The spectra resulted from W4f, W4d, C1s,W4p and O1s could be observed in Fig.3. The bind energies at 35.15 and 37.25 eV were correspond to W $4f_{7/2}$ and W $4f_{5/2}$ orbital, respectively. It is consistent with W(VI) in WO_3/C composite.

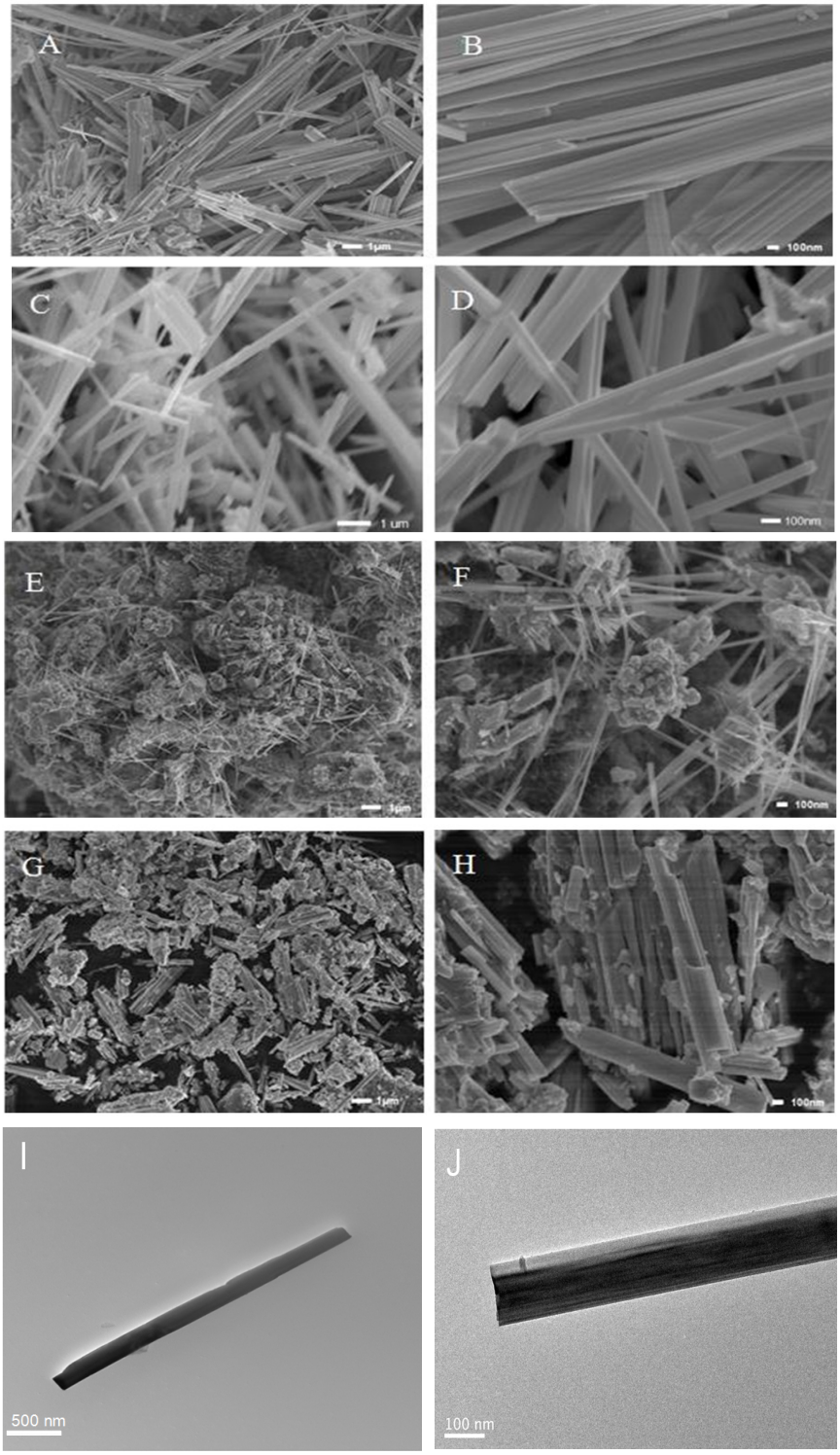

Fig 4. SEM patterns of the four samples: WO_3(A,B), WO_3/C-10(C,D), WO_3/C-20(E,F) and WO_3/C-30(G,H), and TEM images of WO_3/C-10(I,J) sample .

Fig 4. presents SEM micrographs of the WO_3, WO_3/C-10, WO_3/C-20 and WO_3/C-30 composites. As shown clearly in Fig 4. , the micrography of pure WO_3 is nanobelts. However, with the increase of the carbon source, the nanobelts become nanorods, and the length of the nanorods gets shorter and more aggregate with the enhance of the carbon content. Meanwhile, the WO_3/C-30 (G,H) samples are consist of aggregate and shorter nanorods. The TEM images of WO_3/C-10 are shown in Fig 4. (I,J). It could be observed that the WO_3/C-10 composite still kept nanorods morphology, which is in agreement with the SEM images shown in Fig 4. (C,D), and the diameter of the nanorod is about 100nm.

3.2. Electrochemical properties

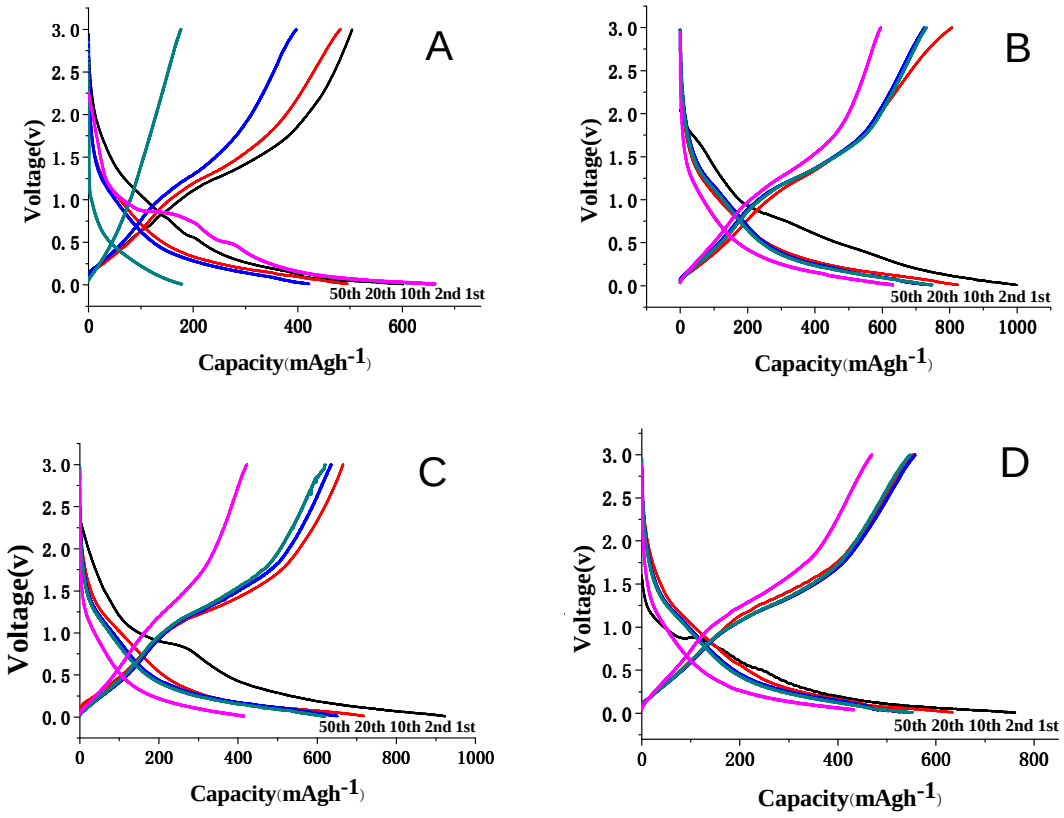

Fig 5. Typical charge/discharge curves of the samples WO_3(A), WO_3/C-10(B), WO_3/C-20(C), WO_3/C-30(D)

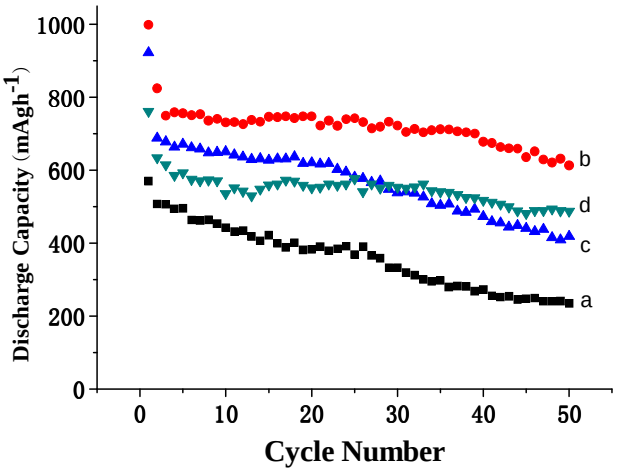

Fig 6. Cycling performance of the: WO_3(a), WO_3/C-10(b), WO_3/C-20(c), WO_3/C-30(d)

The electrochemical performances of the WO_3 samples were measured via coin cell testing. Fig 5. shows the charge and discharge cycle profiles of the electrodes at a current density of 50 mA g^{-1} in the voltage range of 0.01~3.0 V at room temperature, respectively. It can be seen that all these discharge curves exhibit one plateau about 0.8V. The initial discharge capacities of the WO_3(A), WO_3/C-10(B), WO_3/C-20(C), WO_3/C-30(D) were 659.6, 998.82, 922.7 and 761 mAh g^{-1} separately.

Cycling performances of the samples at a current density of 50 mA g^{-1} are shown in Fig 6. It is obvious that the WO_3/C-10(b), WO_3/C-20(c), WO_3/C-30(d) shows much improved electrode performance with higher specific capacities at the same cycle with the same current density, as compared with the WO_3 samples. From these, a large irreversible capacity at the first cycle is observed. The specific capacity of the WO_3 and WO_3/C-20 showed an obvious decrease with cycling, from 659 and 922 mAh g^{-1} for the first cycle to 178 and 414.9 mAh g^{-1} for the 50th cycle, respectively. The WO_3/C-10 delivers a larger initial capacity of 998.82 mAh g^{-1} and shows a high reversible capacity of 807 mAh/g for the second cycle. It still retains a high capacity of 631.25 mAh g^{-1} after 50 cycles.

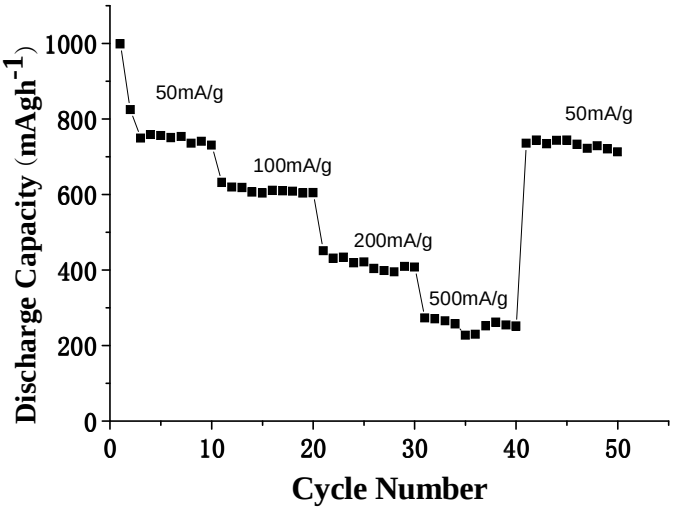

Fig 7. The cycling performance of the WO_3/C-10 electrode at various current densities.

To better understand the electrochemical behavior of the WO_3/C-10 nanorods, we also investigated its rate performance as shown in Fig 7. The WO_3/C-10 electrode was cycled at various current densities (50-500 mA g^{-1}). The cell shows good rate capability with average discharge capacity of 779.83, 611.75, 417.13and 254.52 mA h g^{-1}, when the current density increased stepwise to 50,100, 200 and 500 mA g^{-1}, respectively. Upon altering the current density back to 50 mA g^{-1}, an average discharge capacity been as high as 731.74 mAh g^{-1} could be recovered. This demonstrates that the WO_3/C-10 nanorods structure has great potential as high-rate anode materials in lithium-ion batteries. The nanocomposite shows obvious improved cyclability and rate capability, which could be due to the unique WO_3/C nanorods architecture. The carbon coated composite could not only effectively enhance transport behavior of electrons but also effectively alleviate the volume expansion of WO_3 during charge/discharge cycles.

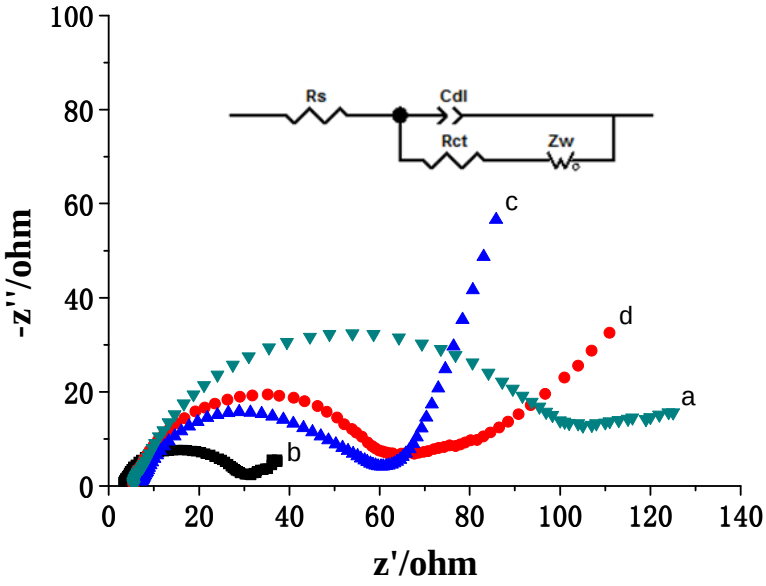

Fig 8. Electrochemical impedance spectra (EIS) of the WO_3(a), WO_3/C-10(b), WO_3/C-20(c) and WO_3/C-30(d).

Fig 8. presents the EIS spectra of the electrodes constructed from the WO_3, WO_3/C-10, WO_3/C-20 and WO_3/C-30 samples synthesized by the hydrothermal method. It can be observed from Fig 8. that the semicircle of the WO_3/C-10, WO_3/C-20 and WO_3/C-30 samples are decreased in comparison with the WO_3 sample, especially the semicircle of the WO_3/C-10, which indicates that the WO_3/C-10 electrode possesses lower contact and charge transfer impedance. Based on the preceding models, every value can be calculated by the non-linear least squares method. The double layer capacitance is modeled by a constant phase element. The charge transfer resistance R_{ct} of the WO_3/C-10, WO_3/C-20 and WO_3/C-30 electrodes are 28.090, 50.62, 67.110Ω/cm^2, which are significantly lower than that for the WO_3(103.10 Ω/cm^2). These facts indicate that WO_3/C would have better electrochemical properties as anode material for lithium-ion batteries.

4. Conclusions

In summary, WO_3/C composite has been successfully synthesized through hydrothermal method. When used as an anode material for LIBs, the as-prepared WO_3/C-10 nanorods show a high specific discharge capacity, good rate capability, and excellent cycling stability. The WO_3/C-10 nanorods electrode behaved an initial capacity of 998.82 mAh g^{-1} at a current density of 50 mA g^{-1}. After 50 cycles, the sample still retained a high capacity of 631.25 mAh g^{-1}. Particularly, WO_3/C-10 nanorods electrode shows good rate capability. The improved electrochemical

performance enables such WO_3 nanorods to be a promising anode material for next-generation, high-power lithium-ion batteries.

Acknowledgments

This work was financially supported by the Hubei Key Laboratory of Pollutant Analysis & Reuse Technology（No.KL2013M08)

References

1. J.O. Besenhard and M. Winter, *Pure & Applied Chemistry.*, **70**, 603-608 (1998).
2. J.M. Tarascon and M. Armand. *Nature*., **414**, 359-367 (2001).
3. Y.A. Shui and Kimagain. *Solid State Ionics*., **100**, 267-273 (1997).
4. J.T. Kloprogge and M.L. Weier, *Materials Chemistry and Physics*., **88**, 438 (2004).
5. J.D. Guo and Y.J. Li, *J. Power Sources*., **54**, 461-464 (1995).
6. K. Huang and Q. Pan, *J. Physics.*, **41**, 417 (2008).
7. R. Wagner and N. Preschitschek, *J. Appl Electrochem*., **43**, 481-496 (2013).
8. T. Ohzuku, R. Brodd. *J. Power Sources*., **174**, 449-456 (2007).
9. D. Deng and M. G. Kim, *Energy Environ*., **2**, 818 (2009).
10. J. S. Chen and L. A. Archer,*J. Mater. Chem.*, **21**, 9912 (2011).
11. J. Cabana and L. *Monconduit, Adv.Mater*., **22**, E170 (2010).
12. Z.J. Gu and H.Q. Li, *J. Solid State Chem.*,**180**, 98 (2007).
13. N. Kumagai and Y. Umetzu, *Solid State Ionics*., **86**, 1443 (1996).
14. W.H. Tao and C.H. Tsai, *Sens. Actuators*., **81**, 237-247 (2002).
15. D. Larcher and G. Sudant, *J. the Electrochemical Society*., **149**, A234 (2002).
16. W. Wang and H.C. Zeng, *Advanced Materials*., **18**, 45 (2006).
17. B. Reichmann and A.J. Bard, *J. the Electrochemical Society*.,**126**, 586 (1979).
18. Y.M. Kang and M.S. Song, *Electrochimica Acta*., **50**, 3667 (2005).
19. J.W. Long and B. Dunn, *White. Chem. Rev*., **104**, 4463 (2004).
20. M.P. Tarassov and M.S. Marinov, *Phys.Chem.Minerals*., **21**, 63-66 (1994).
21. G.N. Kustova and Y.A. Chesalov, *Vibr. Spectr*., **55**, 235-240 (2011).
22. S.H. Lee and H.M. Cheong, *J. Appl. Phys*., **88**, 3076-3078 (2000).
23. N. Kumagai and N. Umetzu, *Solid State Ionics*., **1443**, 86-88 (1996).
24. Z.J. Gu and H.Q. Li, *J. Solid State Chemistry*., **98**, 180 (2007).
25. W. Li and F. Cheng, *J. Physical Chemistry*., **119**, B110 (2006).
26. J.S. Chen and Y.L. Cheah, *J. Physical Chemistry*., **8675**, C114 (2010).